SusTEM2019
https://research.ncl.ac.uk/thermal_challenge_network/

Modelling and performance analysis of heat exchangers for supercritical CO_2 power systems

*Lei Chai *, Savvas A Tassou*

RCUK Centre for Sustainable Energy Use in Food Chain (CSEF), Institute of Energy Futures, Brunel University London, Uxbridge, Middlesex UB8 3PH, UK
* Corresponding author. Email: Lei.Chai@brunel.ac.uk; Tel. +44 (0)1895 265834

Abstract

Heat exchangers are critical components in supercritical CO_2 power systems and can significantly influence the overall system efficiency and size. Microtube, printed circuit and plate heat exchangers are emerging as the most promising technologies for the heater, recuperator and cooler respectively. The heat source is normally exhaust gas and heat rejection is normally to water. The distributed (segment by segment) modelling approach and the *ε-NTU* method were used for the development of simulation models for these heat exchangers. The heat transfer and pressure drop data of each segment are calculated using empirical correlations for Nusselt number and friction factor for each heat exchanger, based on the typical operating conditions of the system. The models were used to characterise the three heat exchangers in terms of heat transfer performance and pressure drop. The present work can provide the basis for the modelling of integrated supercritical CO_2 heat to power systems, and for overall system design optimisation.

Keywords: Modelling; heat transfer; pressure drop; heat exchanger; supercritical CO_2; power system

Nomenclature

A	cross-sectional area of flow, m^2	u_∞	incoming free stream velocity, m/s
c_p	specific heat, J/(kg K)	U	overall heat transfer coefficient, W/(m^2 K)
C	heat capacity rate, W/K	w	width, m
D	hydraulic diameter, m; diameter, m	Δp	pressure drop, Pa
f	friction factor	x	length, m
G	mass flux, kg/(m^2 s)	Greek letters	
h	heat transfer coefficient, W/(m^2 K); height, m	β	herringbone angle, °
k	thermal conductivity, W/(m K)	λ	enlargement factor
m	exponent parameter	ρ	density, kg/m^3
$\dot{m}$	mass flow rate, kg/s	μ	dynamic viscosity, Pa·s
N	total segment number	ε	effectiveness
NTU	number of transfer unit	Subscripts	
Nu	Nusselt number	c	cold
p	pressre, Pa; exponent parameter	h	hot
P	wetted perimeter of cross section, m	i	segment number
Pr	Prandtl number	in	inlet
Q	heat transfer rate, W	max	maximum
R	thermal resistance, K/W	min	minimum
Re	Reynolds number	n	normal direction
S_n	spacing in normal direction, m	p	parallel direction
S_p	spacing in parallel direction, m	s	stainless steel
T	temperature, K	out	outlet
u	velocity, m/s	w	wall

1 Introduction

Due to the globally increasing demand for electrical energy and growing environmental concerns, the supercritical CO_2 Brayton cycle has recently been gaining increased attention for power generation, especially where heat-source temperatures are in the range between 400 and 900 °C, such as for concentrated solar power, fossil fuel power generation and nuclear reactors – even fusion reactors [1-4]. The Supercritical CO_2 power system offers the potential for improved economics in heat to power conversion due to their small size, use of standard materials, and their improved electrical-power-conversion efficiency. Since 2004, Sandia National Laboratories in the USA have been working on the development of supercritical CO_2 Brayton cycle power system. A prototype system has the capability of thermal energy input from 260 kW to 780 kW [5, 6]. Knolls Atomic Power Lab in the USA and the Institute of Applied Energy in Japan have also been developing and testing supercritical CO_2 integrated systems alongside the development of important components such as turbomachinery and heat exchangers [1]. In such systems, heat exchangers play a critical role. This is primarily due to the need to maintain cycle compactness and ensure safe operation at high temperatures and pressures and large differences between the high and low pressure sides of the system. These harsh operating conditions pose significant mechanical, thermomechanical, and thermohydraulic challenges [5].

For heat exchangers used in supercritical CO_2 Brayton cycles, only a few researchers focused on test facilities and experimental work. Nikitin et al. [7] investigated the heat-transfer and pressure-drop characteristics of the printed circuit heat exchanger (PCHE) used as recuperator in a supercritical CO_2 loop and suggested that the PCHE was a promising

compact heat exchanger for this application. Ngo et al. [8] tested the thermohydraulic characteristics of microchannel heat exchangers with S-shaped and zigzag fins for the supercritical CO_2 cycle. They found that both types of heat exchanger had higher heat-transfer performance than either plate fin or circular tube heat exchangers. The Nusselt number of the PCHE with zigzag fins was found to be 34% higher than that of the S-shaped fins, but with the penalty of 4–5 times higher pressure drop. Fourspring et al. [9] described two compact heat-transfer surfaces in the form of two recuperators. One employed a wire mesh as the extended heat-transfer surface, and the other a folded-wavy-fin as the extended heat-transfer surface. Thermohydraulic performance testing showed that the compact recuperator employing the traditional, folded-wavy-fin heat-transfer surface achieved the design heat-transfer rate with less than half the pressure drop.

Lee and Kim [10] used numerical investigations and modelling, to estimate the global Nusselt number, Colburn *j*-factor, effectiveness, and friction factor of a PCHE with various zigzag channel cross-sectional shapes and configurations. Results showed that the rectangular cross section had the best thermal performance but the worst hydraulic performance, while the circular cross section presented the worst thermal performance. Xu et al. [11] investigated a heat exchanger with discontinuous airfoil fins for supercritical CO_2 cycle application and studied the effects of the fin arrangement on heat transfer and flow resistance. Results showed that a sparser, staggered, arrangement of fins can lead to a better thermohydraulic performance. Guo and Huai [12, 13] developed a model of a PCHE recuperator with straight channels employing the segmental design and the ε-*NTU* method and demonstrated their thermohydraulic performance through the entropy generation rate of heat transfer and pressure drop. Chai and Tassou [14] employed the standard k-ε model to investigate the thermohydraulic performance of supercritical CO_2 in a PCHE recuperator with straight channels and compared the local heat transfer and pressure drop results with the predictions from empirical correlations of Nusselt number and friction factor.

Considering their key function and compatibility requirement, the selection and design of heat exchangers are particularly important in the supercritical CO_2 power system (A recuperated cycle is shown in Fig. 1). For the heater, the high-pressure supercritical CO_2 flows inside the channels or tubes, and the high-temperature low-pressure exhaust gas or hot air crosses the channels or tubes [15, 16]. After capital cost evaluation of the supercritical CO_2 power system, Fleming et al. [17] suggested that the use of a lower efficiency and less costly heat exchanger may make this technology more attractive for commercialization, and Chordia et al. [18] recommended the microtube heat exchanger due to its potential to meet the high temperature and high differential pressure criteria but with much lower capital costs. Therefore, a four-module microtube heat exchanger is designed in this paper for the heater. For the recuperator, the supercritical CO_2 works at high pressure, high temperature and high pressure differentials between the exchanging fluids. Among the various types of heat exchangers, the Heatric PCHE with zigzag channels has been selected for the application due to its favourable attributes under conditions of high pressure and temperature [5-8]. For the cooler, the supercritical CO_2 approaches the critical point at the outlet and works in the near-critical region rejecting the heat from the cycle. The brazed plate heat exchanger can withstand high pressure and provide excellent thermal-hydraulic performance and with much lower capital costs [19]. So the chevron-type plate heat exchanger with cooling water is selected and studied in the present work. To investigate the heat transfer and fluid flow processes of supercritical CO_2 in these different types of heat exchangers, distributed modelling and the ε-*NTU* method were used for the heater, recuperator and cooler, respectively.

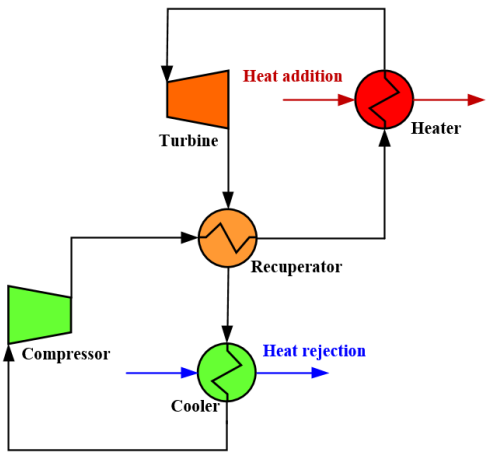

Figure 1: A recuperated supercritical CO_2 power system

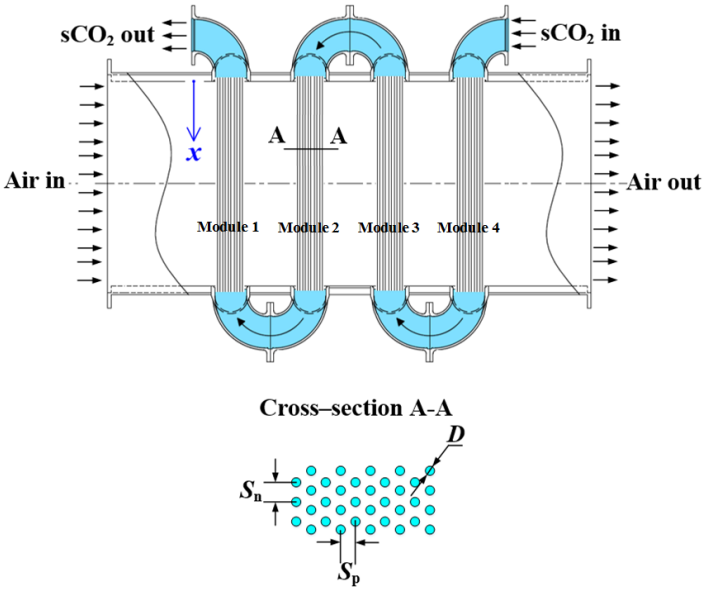

Figure 2: Geometry of heater

2 Description of candidate heat exchangers

Figure 2 illustrates the geometry of the heater. The heater contains four modules of staggered microtube banks. Each module has 1000 microtubes, which are uniformly distributed in 10 rows. The outer tube diameter D is 2 mm, the tube wall thickness is 0.1 mm. The tube spacing in normal direction S_n and in parallel direction S_p are 3.5 mm and 4 mm respectively. The tube material is stainless steel and the tube length is 0.5 m. Supercritical CO_2 flows inside the microtubes, and hot air crosses the tubes in the shell side.

Figure 3 shows the geometry of the recuperator. The recuperative heat exchanger contains a total of 2000 zigzag channels (1000 in cold side and 1000 in the hot side). The configuration parameters are from Ngo et al. [8]. The geometry parameters are the same for the cold and hot sides. The plate thickness is 1.5 mm, the channel spacing in the normal direction S_n and in parallel direction S_p are 3.426 mm and 7.565 mm respectively. The fin angle to the parallel direction θ is 52°, and the zigzag fin width, depth and gap are 0.8, 0.94 and 1.31 mm respectively. High-pressure and low-pressure supercritical CO_2 flow in the cold and hot sides of the recuperator.

Figure 4 presents the geometry of the cooler. The chevron-type plate heat exchanger contains a total of 2000 channels (1000 on cold side and 1000 on hot side). The configuration parameters are from Yang et al. [19]. The plate thickness is 0.4 mm, the corrugation depth b is 2 mm, the herringbone angle β is 65°, and the corrugation pitch λ is 7 mm. The enlargement factor of this chevron plate (ratio of the real area to the projected area) is 1.16, and the corrugation profile aspect ratio is 0.571. Cooling water and supercritical CO_2 flow in the cold and hot sides of the cooler respectively.

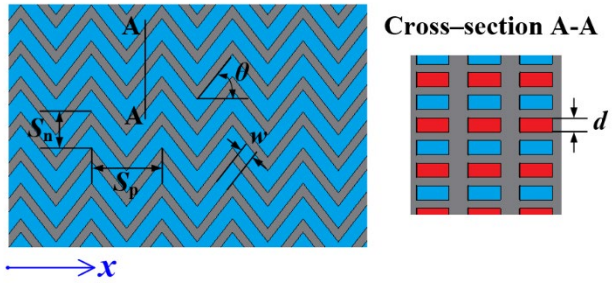

Figure 3: Geometry of recuperator

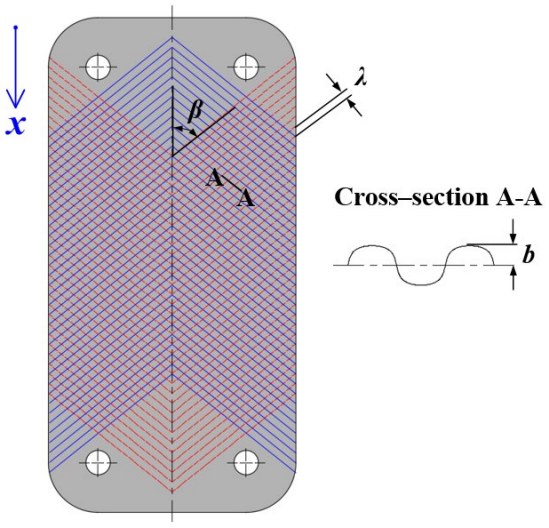

Figure 4: Geometry of cooler

3 Modelling description

The distributed method is employed in the modelling of the different types of heat exchangers. Fig. 5 demonstrates the segment design for a single module of heater with cross flow, and Fig. 6 shows the segment design used for both recuperator and cooler with counter flow. In the present study, as $N > 40$ for a single module of heater and $N > 80$ for both recuperator and cooler, the change of both heat transfer and pressure drop data are less than 1%. Considering the easier data reduction, $N = 50$, 100 and 100 are used for the modelling of the heater, recuperator and cooler respectively. For each uniformly divided segment, the ε-NTU method is employed for the heat transfer and pressure drop calculations. The thermophysical properties of the working fluid in a single segment are assumed to be constant. The properties are obtained by linking NIST REFPROP v9.1.

The ε-NTU method for the heat exchanger analysis was proposed by London and Seban [20]. In this method, the heat transfer rate from the hot fluid to the cold fluid for a given segment i is expressed as,

$$Q_i = \varepsilon_i C_{\min,i} (T_{h,i} - T_{c,i}) \tag{1}$$

where Q is the heat transfer rate, ε is the heat exchanger effectiveness, C is the capacity rate, T_h and T_c are the temperatures in the cold and hot sides respectively.

$$\varepsilon_i = \frac{1 - \exp[-NTU_i(1 - C_i^*)]}{1 - C_i^* \exp[-NTU_i(1 - C_i^*)]} \tag{2}$$

where NTU is the number of transfer units,

$$NTU_i = \frac{U_i A_i}{C_{\min,i}} \tag{3}$$

$$C_i^* = \frac{C_{\min,i}}{C_{\max,i}} \tag{4}$$

$$C_{\min,i} = \min(\dot{m}_{c,i} c_{pc,i}, \dot{m}_{h,i} c_{ph,i}) \tag{5}$$

$$C_{\max,i} = \max(\dot{m}_{c,i} c_{pc,i}, \dot{m}_{h,i} c_{ph,i}) \tag{6}$$

where U is the overall heat transfer coefficient,

$$U_i A_i = \frac{1}{\frac{1}{h_{c,i} A_{c,i}} + R_{s,i} + \frac{1}{h_{h,i} A_{h,i}}} \tag{7}$$

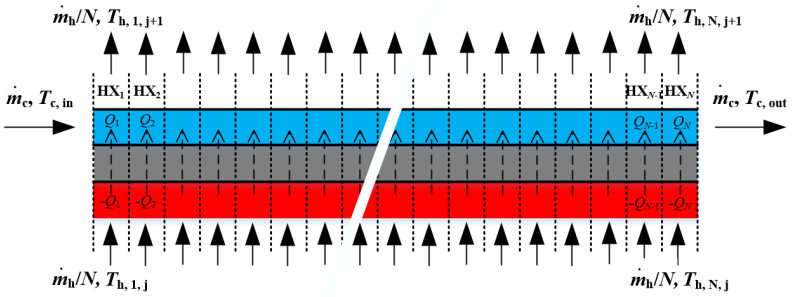

Figure 5: Segment design for a single module of heater with cross flow

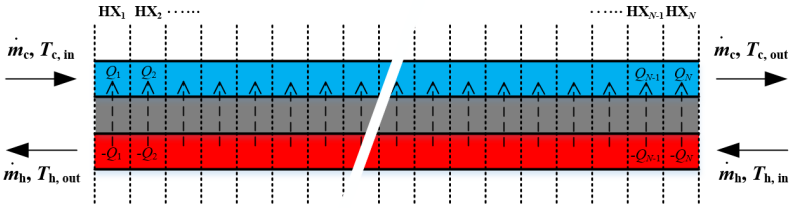

Figure 6: Segment design for recuperator and cooler with counter flow

The thermohydraulic performance of the fluid flowing over or through the channels or tubes is calculated using empirical correlations for Nusselt number and friction factor for each type of heat exchanger. The heat transfer coefficient and friction factor of supercritical CO_2 on the cold side of the heater are computed using the Gnielinski correlations [21],

$$Nu_{c,i} = \frac{(f_{c,i}/8)(Re_{c,i} - 1000)Pr_{c,i}}{1 + 12.7(f_{c,i}/8)^{1/2}(Pr_{c,i}^{2/3} - 1)} \tag{8}$$

$$f_{c,i} = (0.790 \ln Re_{c,i} - 1.64)^{-2} \tag{9}$$

The heat transfer coefficient and friction factor of hot exhaust gas on the hot side of the heater are calculated from Zukauskas [22],

$$Nu_{h,i} = C Re_{d,max}^{n} Pr^{0.36} \left(\frac{Pr}{Pr_w}\right)^{1/4} \tag{10}$$

$$f' = \left\{0.25 + \frac{0.118}{[(S_n - d)/d]^{1.08}}\right\} Re_{max}^{-0.16} \tag{11}$$

where Re_{max} is calculated based on the maximum flow velocity,

$$u_{max} = \frac{u_\infty (S_n/2)}{\left[(S_n/2)^2 + S_p^2\right]^{1/2} - d} \tag{12}$$

where u_∞ is the incoming free stream velocity.

The heat transfer coefficient and friction factor of supercritical CO_2 flowing through the recuperative PCHE with zigzag channels were obtained from Ngo et al. [8]. The correlations were developed for a very similar heat exchanger geometry as the one studied in the present work,

$$Nu_i = 0.1696 Re_i^{0.629} Pr_i^{0.317} \tag{13}$$

$$f_i = 0.1924 Re_i^{-0.091} \tag{14}$$

The heat transfer coefficient and friction factor of cooling water in the chevron-type plate heat exchanger are obtained from Wanniarachchi et al. [23],

$$Nu_i = [Nu_{i,l}^3 + Nu_{i,t}^3]^{1/3} Pr^{1/3} \left(\frac{\mu_i}{\mu_{w,i}}\right)^{0.17} \tag{15}$$

$$Nu_{i,l} = 3.65\beta^{-0.455}\phi^{0.661} Re_i^{0.339} \tag{16}$$

$$Nu_{i,t} = 12.6\beta^{-1.142}\phi^{1-m} Re_i^{m} \tag{17}$$

$$m = 0.646 + 0.0011\beta \tag{18}$$

$$f_{i,p} = [f_{i,l}^3 + f_{i,t}^3]^{1/3} \tag{19}$$

$$f_{i,l} = 1774\beta^{-1.026}\phi^2 Re_i^{-1} \tag{20}$$

$$f_{i,t} = 46.6\beta^{-1.08}\phi^{1+p} Re_i^{-p} \tag{21}$$

$$p = 0.00423\beta + 0.0000223\beta^2 \tag{22}$$

The above mentioned Re_i and D are respectively defined as:

$$Re_i = \frac{GD}{\mu_i} \tag{23}$$

$$D = \frac{4A}{P} \tag{24}$$

where G is the mass flux, A is the cross-sectional area of the flow, and P is the wetted perimeter of the cross section.

Since the density of supercritical CO_2 undergoes a significant change with temperature, practically in the near-critical region, the pressure drop of these three heat exchangers in the cold side $\Delta p_{c,i}$ and in the hot side $\Delta p_{h,i}$ considering the flow acceleration and deceleration can be determined from:

$$\Delta p_{c,i} = \frac{f_{c,i} G_c^2 L}{2\rho_{c,i} DN} + \frac{G_c^2}{2\rho_{c,i}} - \frac{G_c^2}{2\rho_{c,i-1}} \tag{25}$$

$$\Delta p_{h,i} = \frac{f_{h,i} G_h^2 L}{2\rho_{h,i} DN} + \frac{G_h^2}{2\rho_{h,i-1}} - \frac{G_h^2}{2\rho_{h,i}} \tag{26}$$

Based on the above equations, the modelling code for each type of heat exchanger was written in FORTRAN. Depending on the operating conditions of the high temperature heat to power conversion facility constructed at Brunel University London [24], the operating parameters for each heat exchanger are carefully selected and input to their individual component models, and the thermohydraulic performance of each heat exchanger determined.

4 Results and discussion

4.1 Verification of the modelling code

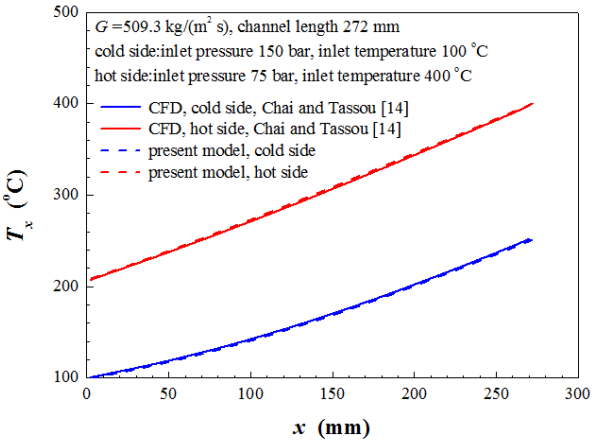

Figure 7: Heat transfer verification

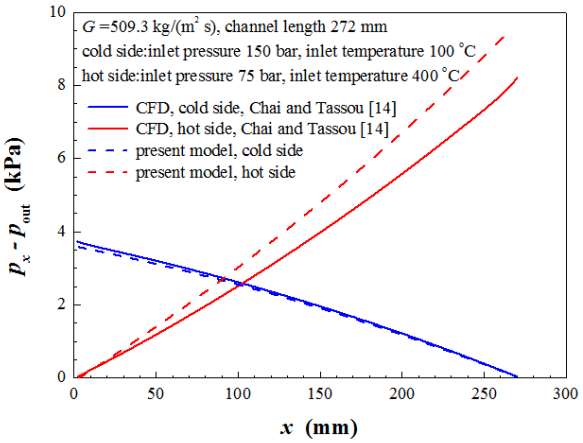

Figure 8: Pressure drop verification

The modelling code of the recuperator was validated by comparing the temperature and pressure distributions of supercritical CO_2 in both cold and hot sides against the computational fluid dynamics (CFD) data from Chai and Tassou [14]. They employed a three-dimensional numerical model that considered real gas thermophysical properties and investigated the thermohydraulic performance of supercritical CO_2 flow in a PCHE recuperator with straight channels. The typical operating conditions and the comparison between the predicted and CFD modelling results are shown in Figs. 7 and 8. It can be seen that the model can predict very well the thermohydraulic performance, except the pressure drop on the hot side at inlet pressure 75 bar, which is a little high but still can be considered acceptable. The higher estimation of pressure drop compared to the CFD result may be from the buoyant effect caused by the much higher temperature difference between the bulk fluid and the wall and the much higher change in thermophysical properties with temperature on the 75 bar pressure side. These comparisons ensure the validation of the modelling codes. Employing widely accepted empirical correlations for supercritical CO_2 in each type of heat exchanger, the modellings of the heater, recuperator and cooler can be valid.

4.2 Performance analysis of the heater

For the supercritical CO_2 power system, the temperature and pressure of the working fluid into the turbine are usually fixed for power generation. In view of the properties of waste heat, the input parameters during the modelling of the heater are designated as $T_{c,out}$ = 500 °C, $T_{h,in}$ = 600 °C, $p_{c,out}$ = 150 bar, $p_{h,in}$ = 1 bar, and the mass flow rate $\dot{m}_{c,out}$ = 1 kg/s and $\dot{m}_{h,in}$ = 1 kg/s. During the modelling, the inlet temperature of hot air for the next segment is assumed to be equal to the outlet temperature of the hot air from the previous segment.

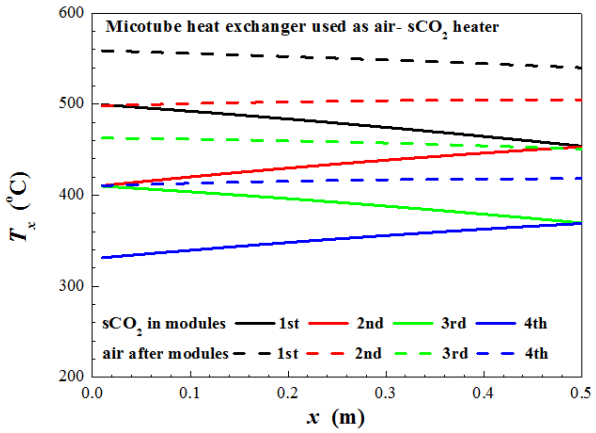

Figure 9: Temperature distribution in the four-module microtube heater

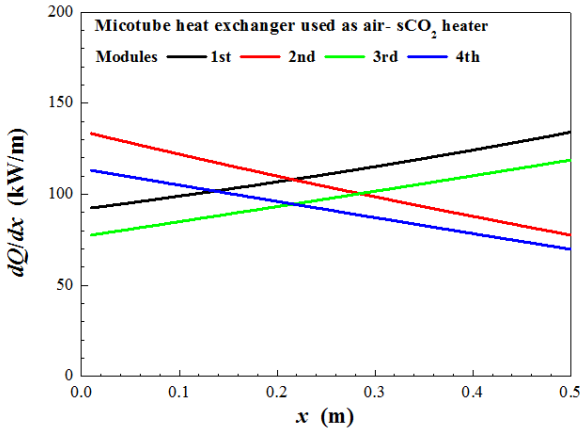

Figure 10: Heat transfer gradient in the four-module microtube heater

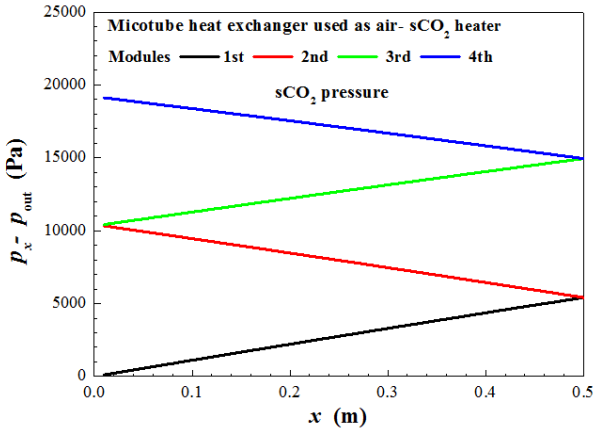

Figure 11: Pressure of supercritical CO_2 in the four-module microtube heater

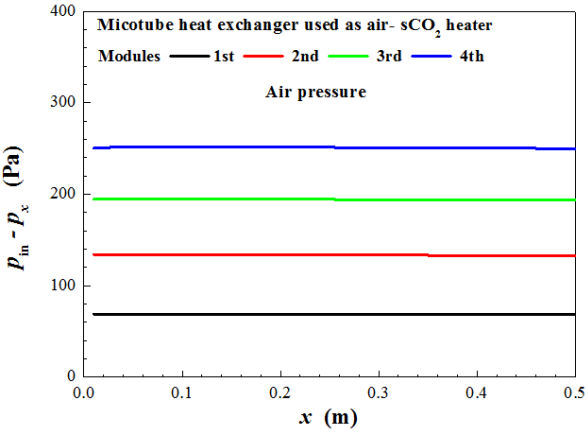

Figure 12: Pressure of air in the four-module microtube heater

Figure 9 shows the temperature variations of supercritical CO_2 in the microtubes and the hot gas after each tube bank module. The temperature of supercritical CO_2 increases along its flow direction. The temperature of the hot gas in the shell side reduces as it flows across the tube banks, and shows less obvious change along the x direction. For the supercritical CO_2, the inlet temperature in each module was calculated as 453.8, 409.8, 369.6 and 331.4 °C. For the hot air, the average outlet temperature after each module is respectively computed as 549.6, 502.2, 457.2 and 414.8 °C. Consequently, the total temperature increase is 168.6 K for the supercritical CO_2 and the total temperature drop is 185.2 K for the hot air in the four-module microtube heater. Fig. 10 indicates the heat transfer gradient for each tube bank module. It can be seen that the heat transfer gradient lies in the range of between 69.8 and 134.1 kW/m, and it increases along the x direction for the first and third modules and drops for the second and fourth modules. The drop is mainly caused by the temperature difference between the supercritical CO_2 and the hot air as shown in Fig. 9. The total heat transfer rate of the present heater is 202.7 kW, with respectively 55.9, 52.1, 48.9 and 45.8 kW for the first, second, third and fourth modules.

Figures 11 and 12 show the pressure distributions of the supercritical CO_2 inside tubes and the hot air after each module. It can be seen that the pressure of supercritical CO_2 continually drops along its flow direction, while the pressure of the hot air drops when crossing the tube bank and the pressure drop is closed to each other for the four modules and the pressure almost does not change along the x direction. The pressure drop of supercritical CO_2 for each module is respectively 5416, 5011, 4616 and 4251 Pa, and the average pressure drop of the hot air for each module is respectively only 68.8, 64.7, 60.6 and 56.8 Pa. Thus the total pressure drop of the supercritical CO_2 is 19.1 kPa on the tube side and that of the hot air is 250.9 Pa on the shell side. The very low pressure drop on the shell side makes this type of heater more suitable for heat addition from high temperature waste heat with low exhaust pressure.

4.3 Performance analysis of the recuperator

For the recuperator in supercritical CO_2 power system, the inlet temperature and pressure of supercritical CO_2 on the cold side are often determined by the thermal and dynamic performance of the compressor and those in the hot side are mostly dependent on the turbine performance. Therefore, the input parameters during the modelling of the recuperator are fixed at $T_{c,in}$ = 100 °C, $T_{h,in}$ = 400 °C, $p_{c,in}$ = 150 bar, $p_{h,in}$ = 75 bar, and the studied balanced mass flow rate is $\dot{m}_{c,in} = \dot{m}_{h,in}$ = 1 kg/s.

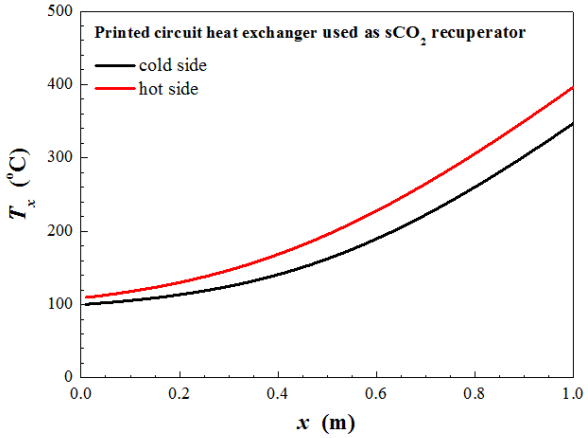

Figure 13: Temperature distribution in the recuperator with zigzag channels

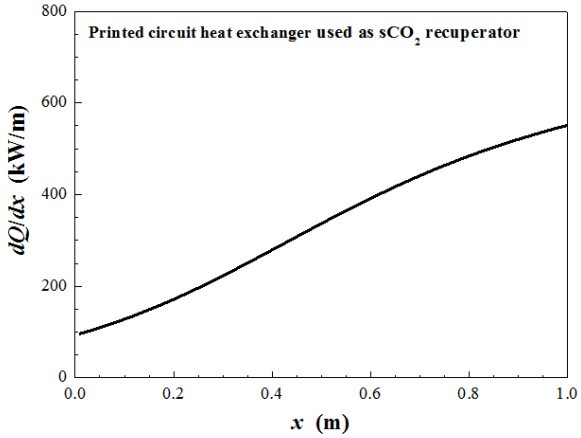

Figure 14: Heat transfer gradient in the recuperator with zigzag channels

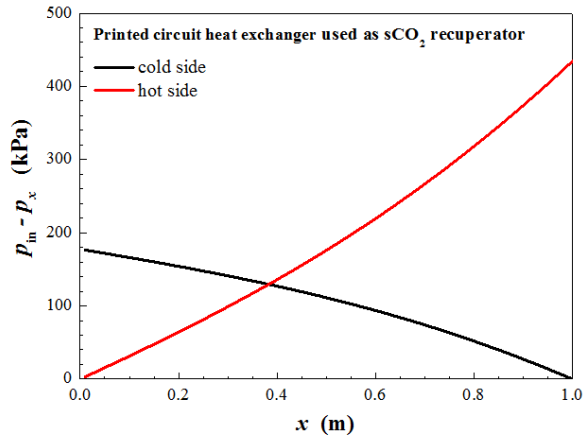

Figure 15: Pressure of supercritical CO_2 in the recuperator with zigzag channels

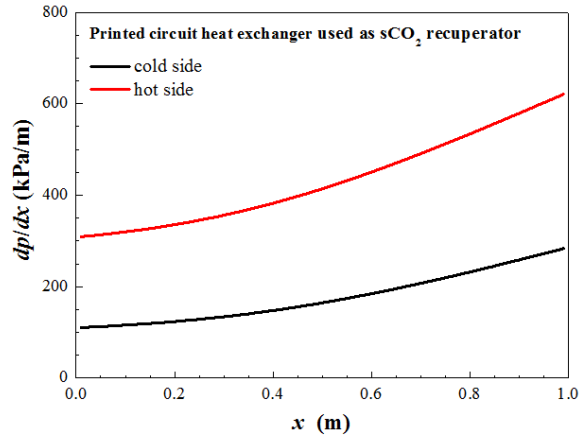

Figure 16: Pressure gradient in the recuperator with zigzag channels

Figure 13 shows the temperature distributions of supercritical CO_2 in both cold and hot sides of the recuperator. It can be seen that the temperature difference between the hot and cold sides increases along the x direction. This is mostly brought about by the different specific heat of supercritical CO_2 under different pressures. The outlet temperature of supercritical CO_2 is 346.9 °C and 109.7 °C on the cold and hot sides respectively. An increased temperature difference results in an increase of heat transfer gradient along the x direction as shown in Fig. 14, which is also dependent on the heat transfer coefficients on both sides. The heat transfer gradient varies in the range from 96.6 to 550.9 kW/m. The total heat transfer rate is 332.1 kW and the corresponding heat exchanger effectiveness is 0.968. Taking the geometry parameters into account, the heat transfer capacity of the PCHE is 33.1 MW/m^3. Its superior heat transfer capacity makes this type of heat exchanger preferable for the recuperator design in supercritical CO_2 power systems, in spite of its high capital cost.

Figures 15 and 16 respectively show the local pressure and pressure gradient of supercritical CO_2 on both cold and hot sides of the recuperator. It can be seen that the pressure gradient in the hot side is much larger than that in the cold side. This is mainly caused by the variation of density, where the density on the cold side is much higher than that on the hot side due to the much higher operating pressure. It can also be seen that the pressure gradient increases with increasing temperature for both sides. An increased temperature leads to an increased dynamic viscosity of supercritical CO_2 under the same pressure, then a decreased Reynolds number and an increased friction factor and thus an increased pressure gradient as equations (25) and (26) show. The total pressure drop of supercritical CO_2 is 177.4 kPa on the cold side and 434.1 kPa on the hot side. The pressure gradient of supercritical CO_2 lies in the range from 110.7 to 287.6 kPa/m on the cold side and from 309.4 to 632.2 kPa/m on the hot side. It can be seen that the zigzag channels cause much larger pressure drop, which should be taken into consideration in recuperator design and selection.

4.4 Performance analysis of the cooler

For the supercritical CO_2 power system, the temperature and pressure of working fluid into the compressor are usually fixed as well as the cooling water temperature. The input parameters during the modelling of the cooler are $T_{c,in}$ = 25 °C, $T_{h,out}$ = 35 °C, $p_{c,in}$ = 1 bar, $p_{h,out}$ = 75 bar, and the mass flow rate $\dot{m}_{c,in}$ = 1 kg/s and $\dot{m}_{h,out}$ = 1 kg/s.

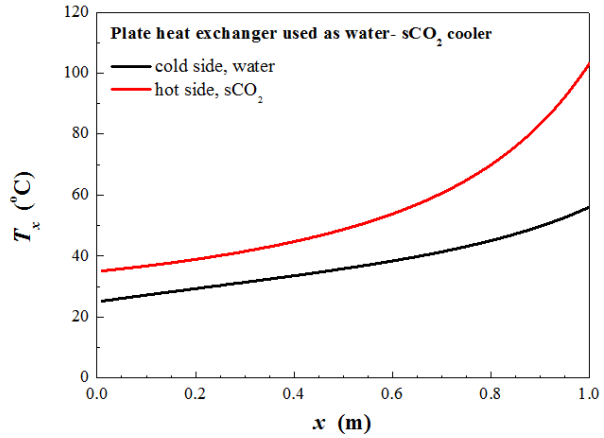

Figure 17: Temperature distribution in the chevron-type plate cooler

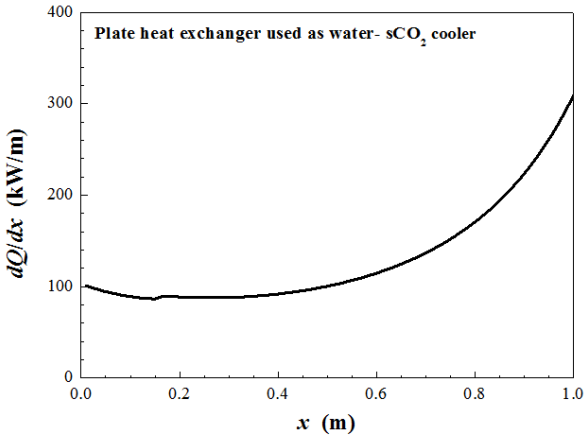

Figure 18: Heat transfer gradient in the chevron-type plate cooler

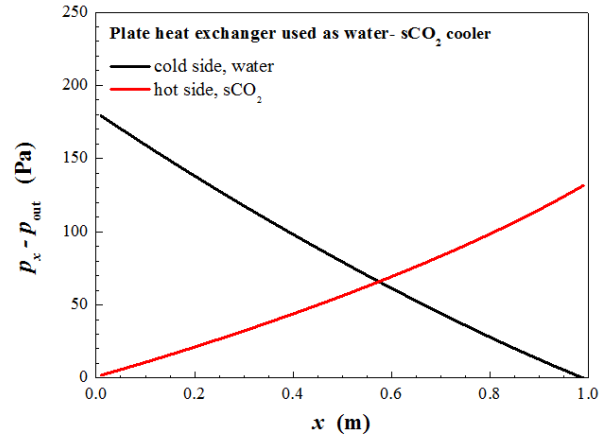

Figure 19: Pressure of supercritical CO_2 in the chevron-type plate cooler

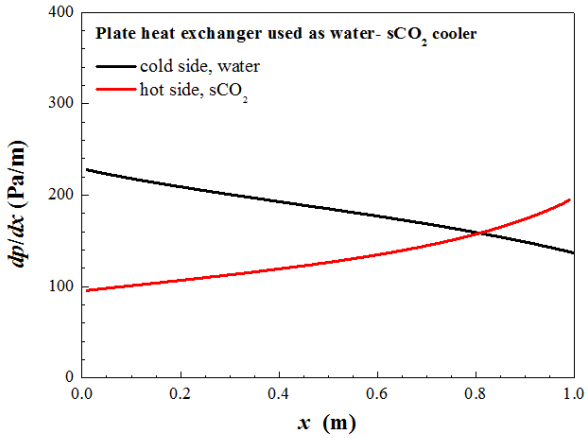

Figure 20: Pressure gradient in the chevron-type plate cooler

Figure 17 shows the temperature variations of supercritical CO_2 on the hot side and cooling water on the cold side of the cooler. The temperature difference between the hot and cold sides firstly changes little and then becomes significantly larger along the x direction (from 10 K at x = 0 to 48 K at x = 1 m). This is mainly caused by the specific heat difference of supercritical CO_2 and cooling water under the operating conditions. The heat transfer gradient along the x direction is presented in Fig. 18, which firstly decreases and then increases quickly. The first decrease is caused by the decreased heat transfer coefficient with increasing temperature for supercritical CO_2 away from the near critical region, and the next rapid increase mainly results from the quick increase of temperature difference between the supercritical CO_2 and the cooling water. The calculated inlet temperature of supercritical CO_2 is 103.1 °C on the hot side and the outlet temperature of water is 55.1 °C on the cold side. The computed total heat transfer rate of this cooler is 130.9 kW.

Figures 19 and 20 illustrate the local pressure and pressure gradient of supercritical CO_2 on the hot side and the cooling water on the cold side. The total pressure drop is 183.8 kPa for the cooling water and 131.7 kPa for the supercritical CO_2. For the cooling water, the pressure gradient experiences a stable decrease along the x direction. This is caused the variation of dynamic viscosity of cooling water, which continually drops with the increase in temperature. The decreased dynamic viscosity leads to increased Reynolds number and decreased friction factor. For the supercritical CO_2, the pressure gradient rises with increased temperature, as a result of the variation of both density and dynamic viscosity. The variation of pressure gradient with temperature of supercritical CO_2 has been analysed in the last section in the investigation of the

performance of the recuperator. The pressure gradient changes from 136.8 to 227.6 kPa/m for the cooling water and from 95.8 to 195.2 kPa/m for the supercritical CO_2.

5 Conclusions

In this paper, a four-module microtube heat exchanger, a PCHE with zigzag channels and a chevron-type plate heat exchanger are modelled as the heater, recuperator and cooler in a supercritical CO_2 power system respectively. Modelling is based on the distributed (segment by segment) approach and the *ε-NTU* method. For each segment, the empirical correlations of Nusselt number and friction factor were carefully chosen for each type of heat exchanger and employed for the heat transfer and pressure drop calculations. The modelling approach was validated by comparing the results with results from CFD modelling and data published in the literature. The modelling codes developed are not only suitable for the heat exchangers presented in this paper, but can be easily be extended to other similar types of heat exchanger with careful selection of the Nusselt number and friction factor correlations.

Based on the model predictions, the following conclusions can be drawn. For the four-module microtube heater, when the inlet temperature and pressure of hot exhaust gas are 600 °C and 1 bar and the outlet temperature and pressure of the supercritical CO_2 are 500 °C and 150 bar, the total heat transfer rate is 202.7 kW, and the total pressure drop is 19.1 kPa for the supercritical CO_2 and 250.9 Pa for the hot gas. For the PCHE recuperator, when the inlet temperature and pressure of supercritical CO_2 are 100 °C and 150 bar on the cold side and 400 °C and 75 bar on the hot side, the total heat transfer rate is 332.1 kW, and the total pressure drop 177.4 kPa on the cold side and 434.1 kPa on the hot side. For the chevron-type plate cooler, when the inlet temperature and pressure of cooling water are 25 °C and 1 bar and the outlet temperature and pressure of supercritical CO_2 are 35 °C and 75 bar, the total heat transfer rate is 130.9 kW, and the total pressure drop is 183.8 kPa for the cooling water and 131.7 kPa for the supercritical CO_2.

The heat transfer and pressure drops in the three heat exchangers have a significant impact on the overall performance of the sCO_2 heat to power system. Using the heat exchanger models, an integrated model of the sCO_2 system can be developed and used for overall system design and optimisation.

Acknowledgements

The work presented in this paper is supported by a number of funders as follows: i) The Engineering and Physical Sciences Research Council (EPSRC) of the UK under research grants EP/P004636/1 'Optimising Energy Management in Industry - OPTEMIN', and EP/K011820/1 (Centre for Sustainable Energy Use in Food Chains) and ii) the European Union's Horizon 2020 research and innovation programme under grant agreement No. 680599, -Industrial Thermal Energy Recovery and Management – I-TERM'. The authors would like to acknowledge the financial support received from the funders and industry partners. All data used are in the paper but if any additional information is required it can be obtained by contacting the corresponding author.

References

1. Ahn Y, Bae S J, Kim M, et al. Review of supercritical CO_2 power cycle technology and current status of research and development. Nuclear Engineering and Technology, 2015, 47(6): 647-661.
2. Manente G, Lazzaretto A. Innovative biomass to power conversion systems based on cascaded supercritical CO_2 Brayton cycles. Biomass and Bioenergy, 2014, 69: 155-168.
3. Linares J I, Herranz L E, Fernández I, et al. Supercritical CO_2 Brayton power cycles for DEMO fusion reactor based on Helium Cooled Lithium Lead blanket. Applied Thermal Engineering, 2015, 76: 123-133.
4. Garg P, Kumar P, Srinivasan K. Supercritical carbon dioxide Brayton cycle for concentrated solar power. The Journal of Supercritical Fluids, 2013, 76: 54-60.
5. Wright S A, Conboy T M, Parma E J, et al. Summary of the Sandia Supercritical CO_2 Development Program. Sandia National Laboratories (SNL-NM), Albuquerque, NM (United States), 2011.
6. Pasch J, Carlson M, Fleming D, et al. Evaluation of recent data from the Sandia National Laboratories closed Brayton cycle testing, ASME Turbo Expo 2016: Turbomachinery Technical Conference and Exposition. American Society of Mechanical Engineers, 2016: V009T36A015-V009T36A015.
7. Nikitin K, Kato Y, Ngo L. Printed circuit heat exchanger thermal–hydraulic performance in supercritical CO2 experimental loop. International Journal of Refrigeration, 2006, 29(5): 807-814.
8. Ngo T L, Kato Y, Nikitin K, et al. Heat transfer and pressure drop correlations of microchannel heat exchangers with S-shaped and zigzag fins for carbon dioxide cycles. Experimental Thermal and Fluid Science, 2007, 32(2): 560-570.
9. Fourspring P M, Nehrbauer J P, Sullivan S, et al. Testing of compact recuperators for a supercritical CO2 Brayton power cycle. Proceedings of the 4th International Symposium on Supercritical CO_2 Power Cycles, 2014.
10. Lee S M, Kim K Y. Comparative study on performance of a zigzag printed circuit heat exchanger with various channel shapes and configurations. Heat Mass Transfer, 2013, 49(7): 1021-1028.
11. Xu X, Ma T, Li L, et al. Optimization of fin arrangement and channel configuration in an airfoil fin PCHE for supercritical CO_2 cycle. Applied Thermal Engineering, 2014, 70(1): 867-875.

12. Guo J. Design analysis of supercritical carbon dioxide recuperator. Applied energy, 2016, 164: 21-27.
13. Guo J, Huai X. Performance analysis of printed circuit heat exchanger for supercritical carbon dioxide. Journal of Heat Transfer, 2017, 139(6): 061801.
14. Chai L, Tassou S A. Numerical study of the thermohydraulic performance of printed circuit heat exchangers for supercritical CO_2 Brayton cycle applications. Energy Procedia, 2019, 161, 480-488.
15. Stehlík P, Jegla Z, Kilkovský B. Possibilities of intensifying heat transfer through finned surfaces in heat exchangers for high temperature applications. Applied Thermal Engineering, 2014, 70(2): 1283–1287.
16. Chai L, Tassou S A. A review of airside heat transfer augmentation with vortex generators on heat transfer surface. Energies, 2018, 11(10): 2737.
17. Fleming D, Pasch J, Conboy T, Carlson M. Testing platform and commercialization plan for heat exchanging systems for SCO_2 power cycles, Proceedings of ASME Turbo Expo 2013: Turbine Technical Conference and Exposition, June 3-7, 2013, San Antonio, Texas, USA
18. Chordia L, Portnoff M A, Green E. High temperature heat exchanger design and fabrication for systems with large pressure differentials, Thar Energy, LLC, Pittsburgh, PA (United States), 2017.
19. Yang J, Jacobi A, Liu W. Heat transfer correlations for single-phase flow in plate heat exchangers based on experimental data. Applied Thermal Engineering, 2017, 113: 1547-1557.
20. London A L, Seban R A. A generalization of the methods of heat exchanger analysis. International Journal of Heat and Mass Transfer, 1980, 23(1): 5-16.
21. Gnielinski V. New equations for heat and mass transfer in turbulent pipe and channel flow. International Chemical Engineering, 1976, 16(2): 359-368.
22. Žukauskas A. Heat transfer from tubes in crossflow. Advances in heat transfer. Elsevier, 1972, 8: 93-160.
23. Wanniarachchi A S, Ratnam U, Tilton B E, et al. Approximate correlations for chevron-type plate heat exchangers. American Society of Mechanical Engineers, New York, NY (United States), 1995.
24. Bianchi G, Saravi S S, Loeb R, Tsamos K M, Marchionni M, Leroux A, Tassou S A. Design of a high-temperature heat to power conversion facility for testing supercritical CO_2 equipment and packaged power units. Energy Procedia, 2019, 161, 421-428.